Author Manuscript

Author Manuscript

Author Manuscript

Author Manuscript

HHS Public Access

Author manuscript

Mol Cancer Res. Author manuscript; available in PMC 2022 October 01.

Published in final edited form as:

Mol Cancer Res. 2022 April 01; 20(4): 501–514. doi:10.1158/1541-7786.MCR-21-0352.

GFI1 cooperates with IKZF1/IKAROS to activate gene expression in T-cell acute lymphoblastic leukemia

Wenxiang Sun[1,2], **Jingtao Guo**[2,3,§], **David McClellan**[2,3], **Alexandra Poeschla**[1], **Diana Bareyan**[2], **Mattie J. Casey**[2,3], **Bradley R. Cairns**[2,3,4], **Dean Tantin**[1,2,*], **Michael E. Engel**[2,3,5,6,Ψ,*]

[1]Department of Pathology, University of Utah School of Medicine, Salt Lake City, UT 84112, USA.

[2]Huntsman Cancer Institute, University of Utah School of Medicine, Salt Lake City, UT 84112, USA.

[3]Department of Oncological Sciences, University of Utah School of Medicine, Salt Lake City, UT 84112, USA.

[4]Howard Hughes Medical Institute, University of Utah School of Medicine, Salt Lake City, Utah.

[5]Department of Pediatrics, University of Utah School of Medicine, Salt Lake City, UT 84112, USA.

[6]Primary Children's Hospital, Salt Lake City, UT 84112, USA.

Abstract

Growth factor independence-1 (GFI1) is a transcriptional repressor and master regulator of normal and malignant hematopoiesis. Repression by GFI1 is attributable to recruitment of LSD1-containing protein complexes via its SNAG domain. However, the full complement of GFI1 partners in transcriptional control is not known. We show that in T-ALL cells, GFI1 and IKAROS are transcriptional partners that co-occupy regulatory regions of hallmark T cell development genes. Transcriptional profiling reveals a subset of genes directly transactivated through the GFI1—IKAROS partnership. Among these is *NOTCH3*, a key factor in T-ALL pathogenesis. Surprisingly, NOTCH3 expression by GFI1 and IKAROS requires the GFI1 SNAG domain but occurs independent of SNAG—LSD1 binding. GFI1 variants deficient in LSD1 binding fail to activate NOTCH3, but conversely, small molecules that disrupt the SNAG—LSD1 interaction while leaving the SNAG primary structure intact stimulate NOTCH3 expression. These results identify a non-canonical transcriptional control mechanism in T-ALL which supports GFI1-mediated transactivation in partnership with IKAROS and suggest competition between LSD1-containing repressive complexes and others favoring transactivation.

[*]**Corresponding authors:** Michael E. Engel, Department of Pediatrics, Division of Pediatric Hematology/Oncology, P.O. Box 800386, University of Virginia School of Medicine, Charlottesville, VA 22908-0386, USA. Phone +1(434)924-5292 or (434)924-5105; Fax +1(434)982-1927; mee2mj@hscmail.mcc.virginia.edu. Dean Tantin, Department of Pathology and Huntsman Cancer Institute, University of Utah School of Medicine, Salt Lake City, UT 84112, USA. Phone +1(801)587-3035; Fax +1(801)585-2417; dean.tantin@path.utah.edu.

[Ψ]Present address: Michael E. Engel, Department of Pediatrics, Division of Pediatric Hematology/Oncology, P.O. Box 800386, University of Virginia School of Medicine, Charlottesville, VA 22908-0386, USA.

[§]Present address: Jingtao Guo, Department of Surgery, Division of Urology, University of Utah School of Medicine, Salt Lake City, UT 84112, USA.

Conflict of interest disclosure statement: The authors declare no conflicts of interest, direct or indirect, associated with this manuscript.

Author Manuscript Author Manuscript Author Manuscript Author Manuscript

Keywords

GFI1; IKAROS; NOTCH3; T-cell Acute Lymphoblastic Leukemia (T-ALL); LSD1

Introduction

Growth factor independence-1 (GFI1) is a zinc finger transcription factor which plays essential roles in normal and malignant myeloid and lymphoid hematopoiesis (1,2). Germline *GFI1* mutations cause severe congenital neutropenia (3), while *Gfi1* null mice show impaired T cell and neutrophil differentiation (4–6). In acute myelogenous leukemia (AML), *GFI1* mRNA expression can be used to stratify patient survival, while *GFI1* displays a dose-dependent impact on the pace of leukemic progression brought on by onco-fusion proteins, MLL-AF9 and NUP98-HOXD13 (7,8). Notably, a GFI1 variant, GFI136N, generated from a single nucleotide polymorphism expressed in 3–7% of the Caucasian population, is disproportionately observed in AML patients and increases risk for AML development by 60% relative to the more common GFI136S variant (9). *GFI1* mRNA is also elevated in samples from patients with early T cell precursor acute lymphoblastic leukemia (ETP-ALL) who display a positive NOTCH signature (10). ETP-ALL is a high-risk subgroup of T-ALL (11), which itself is an aggressive form of acute leukemia characterized by the expansion of immature lymphoid precursor cells (12). The precise role of GFI1 in T-ALL is not clear.

T-ALL has a high incidence of relapse, and survival following disease recurrence is dismal. Aberrant activation of NOTCH signaling is a unifying theme in T-ALL, and arises either from mutations in NOTCH receptors or NOTCH regulators. Normally, in response to ligand binding, NOTCH receptors are cleaved by γ-secretase to liberate their intracellular domains (NICD). NICD then partners with nuclear factors to direct the expression of canonical NOTCH target genes. *NOTCH1*-activating mutations are found in approximately 60% of T-ALL cases. While γ-secretase inhibitors (GSIs) have shown anti-leukemic activity *in vitro* and in murine models, they have not been integrated into T-ALL treatment protocols because of dose-limiting gastrointestinal toxicity and poor anti-leukemic efficacy (13). Like NOTCH1, NOTCH3 promotes T cell lineage specification and leukemogenesis. *NOTCH3*-activating mutations have been identified in approximately 5% of T-ALL cases and NOTCH3 blocking antibodies exhibit potent anti-leukemic effect in T-ALL (14–16). Moreover, abnormal expression and/or activation of *NOTCH3* is seen in T-ALL patient samples lacking *NOTCH1*-activating mutations, reinforcing NOTCH signaling as critical for T-ALL pathogenesis and suggesting *NOTCH3* and factors controlling its expression could represent alternative therapeutic targets in this disease (17,18). The development of new strategies for T-ALL treatment depends upon deeper understanding of its molecular underpinnings.

Here, we identify IKAROS, expressed by the *IKZF1* gene, as a frequent DNA binding partner for GFI1. GFI1 and IKAROS do not interact in classical co-immunoprecipitation (co-IP) assays, but their proximity relationship is impaired by the N383S mutation that impairs GFI1 DNA binding and the N159A mutation that impairs IKAROS DNA binding.

Author Manuscript Author Manuscript Author Manuscript Author Manuscript

In contrast, their interaction is not affected by LSD1 binding-deficient GFI1 variants. We identify a strong, genome-wide correlation between GFI1- and IKAROS-regulated genes through ChIP-Seq. Genes co-occupied by GFI1 and IKAROS encode hallmark T cell development proteins such as NOTCH3, CD3, GFI1 itself, MYC, MYB and HES1. Gene expression profiling by RNA-Seq identifies a cluster of genes activated by ectopic GFI1 expression and repressed with IKAROS knockout. Interestingly, these genes include the direct GFI1/IKAROS target *NOTCH3,* a critical oncogenic factor in T-ALL. Using CCRF-CEM, SUP-T1 and Jurkat T-ALL cells, we show that inducible expression of either GFI1 or IKAROS elevates NOTCH3 cell surface expression, while acute degradation of IKAROS or CRISPR/Cas9-mediated IKAROS knockout significantly attenuates GFI1-mediated NOTCH3 induction. GFI1-dependent stimulation of NOTCH3 cell surface expression depends upon SNAG domain amino acids that enable interaction with LSD1. Yet, LSD1 inhibition and disruption of the SNAG—LSD1 interaction augments *NOTCH3* expression, suggesting that LSD1 competes with co-activators for access to the GFI SNAG domain. Together, these results identify a non-canonical transactivation mechanism for GFI1, working in partnership with IKAROS to promote expression of *NOTCH3* and related T cell development genes, and providing new insights for therapeutic targeting in T-ALL.

Materials and Methods

Cells and Culture conditions

Both CCRF-CEM (ATCC Cat# CRM-CCL-119, RRID:CVCL_0207) and SUP-T1 (ATCC Cat# CRL-1942, RRID:CVCL_1714) were cultured in RPMI 1640 medium, 10% fetal bovine serum, 2 mM GlutaMAX-I, 100 U/mL penicillin and 100 μg/mL streptomycin. Cell lines authentication was performed by ATCC. Cultured cells were passaged ten or fewer times from frozen stocks maintained in liquid nitrogen after cells were expanded at the time of purchase from ATCC. Mycoplasma testing was routinely performed by PCR. All cell culture materials were obtained from ThermoFisher Scientific, Waltham, MA.

Antibodies and Flow Cytometry

Antibodies used for immunoblotting and immunoprecipitation were as follows: LSD1 (Cell Signaling Technology Cat# 2184, RRID:AB_2070132); CoREST (Cell Signaling Technology Cat# 14567, RRID:AB_2798514); IKAROS (Thermo Fisher,Scientific Cat# PA5–23728, RRID:AB_2541228);β-actin (Santa Cruz Biotechnology Cat# sc-47778 HRP, RRID:AB_2714189); α-tubulin (Santa Cruz Biotechnology Cat# sc-5286, RRID:AB_628411); FLAG antibody (Sigma-Aldrich Cat#F1804, RRID:AB_262044); HA antibody (Sigma-Aldrich Cat#11583816001, RRID:AB_514505). Streptavidin-HRP was purchased from GE Healthcare (Cat# RPN1231). All flow cytometric data collection used a BD LSRFortessa flow cytometer. Antibodies used for flow cytometry were APC anti-human NOTCH3 (BioLegend,Cat#345410, RRID:AB_2564483), APC mouse IgG1, Isotype Ctrl antibody (BioLegend, Cat#400119, RRID:AB_2888687) and PE Mouse Anti-Human CD3 (BD, Cat#347347, RRID:AB_400287)

Author Manuscript Author Manuscript Author Manuscript Author Manuscript

Constructs and Cloning

In-frame GFI1 fusion proteins with BirA* were created by subcloning GFI1 from constructs in our previous study (19) into the *Eco*RI and *Bam*HI sites of the MCS-BioID2-HA vector (a gift from Dr.Kyle Roux, University of South Dakota, RRID:Addgene_74224). Subsequently, GFI1-BirA*-HA PCR products were cloned into the *Not*I and *Eco*RI sites of the pLVX-Tight-Puro vector (Clontech Laboratories, Inc). We used the rat GFI1 ortholog for our experiments, which is >99% conserved at the amino acid level with human GFI1. *IKZF1*/IKAROS expression constructs were based on the human form. The N383S derivative of rat GFI1 is analogous to the N382S mutation in human GFI1.

Lentivirus Packaging

To generate lentiviral particles, HEK293T cells were transfected with lentiviral packing vectors, viral packaging (psPAX2, RRID: Addgene_12260) and viral envelope (pMD2.G, RRID:Addgene_12259) constructs at a 4:2:1 ratio with 1 mg/mL polyethylenimine (Sigma-Aldrich Cat # 408727). The ratio of total transfected DNA to PEI was 1:3 (1 μg DNA:3 μg PEI). After 24 hr, 20 mL of fresh cell culture medium was added and the cells were incubated for an additional 24 hr. Then the culture medium was replaced with virus collection medium (culture medium with 20mM HEPES). Viral supernatants were collected after a further 8 and 24hr. The two supernatants were combined and passed through a 0.45μm filter. Virus was directly used for infection or stored at −80°C.

BioID proximity purification and proteomic analysis (MassIVE File Identifier MSV000086405)

CCRF-CEM cells were transduced with Tet-On lentiviral vectors (Lenti-XTM Tet-On Advanced, Clontech Laboratories, Inc) and selected with 500 μg/mL G418 to generate CCRF-CEM-Tet-On cells. CCRF-CEM-Tet-On cells were transduced with empty vector, BirA*-HA or GFI1-BirA*-HA viruses (pLVX-Tight-Puro, pLVX-Tight-puro-BirA*-HA or pLVX-Tight-Puro-GFI1-BirA*-HA, respectively) and selected with 0.5 μg/mL puromycin to generate CCRF-CEM cells expressing doxycycline-inducible GFI1-BirA* fusion proteins or BirA*. Cells were treated with 1 μg/mL doxycycline for 48 hr and 20 μM biotin for 16 hr. Cells were lysed in buffer (50 mM Tris-HCl pH 7.5, 500 mM NaCl, 0.5 mM EDTA, 1% Triton X-100) and incubated with streptavidin-Sepharose High Performance beads (Sigma, GE17–5113-01) on ice for 16hr. After washing the beads five times with lysis buffer on ice, proteins were eluted with 2× Laemmli Sample Buffer (LSB, 65.8 mM Tris-HCl pH 6.8, 26.3% (w/v) glycerol, 2.1% SDS, 0.01% bromophenol blue) and boiled for 10 min. Proteins were resolved by SDS-PAGE. Whole lanes of SDS-PAGE gels were excised and subjected to LTQ Orbitrap Velos Pro ion-trap mass spectrometry (ThermoFisher Scientific, Waltham, MA). Peptides were detected, isolated, and fragmented to produce a tandem mass spectrum of specific fragment ions for each peptide. Protein identity was determined by matching protein databases with the acquired fragmentation pattern using Sequest software (ThermoFisher Scientific, Waltham, MA). All databases include a reversed version of all the sequences and the data was filtered to a 1–2% peptide false discovery rate.

Author Manuscript Author Manuscript Author Manuscript Author Manuscript

ChIP-Seq (Gene Expression Omnibus Series record GSE160183) and ChIP qPCR

The CCRF-CEM-Tet-On cells described above were infected with GFI1–3×FLAG or IKAROS-3×FLAG viruses (packaged with pLVX-Tight-puro-GFI1–3×FLAG or pLVX-Tight-puro-IKAROS-3×FLAG plasmids). Cells were selected with 1μg/mL puromycin to produce CCRF-CEM stable cell lines inducibly expressing GFI1–3×FLAG and IKAROS-3×FLAG. These cells were treated with 1μg/mL doxycycline for 24 hr. 20 million CCRF-CEM cells were cross-linked using a final concentration of 1% formaldehyde in the medium for 10 min. Cross-linking was quenched with 0.125 M glycine for 2 min. Cells were washed with ice-cold PBS and Farnham lysis buffer (5 mM PIPES pH 8.0, 85 mM KCl, 0.5% NP-40, 1 mM PMSF and 10μg/mL Aprotinin). Cells were resuspended in 1 mL RIPA lysis buffer (1X PBS, 1% NP-40, 0.5% sodium deoxycholate, 0.1% SDS, 1 mM PMSF and 10 μg/mL Aprotinin). Cells were sonicated to shear the DNA to between 200 and 500 bp. 50 μL of sonicated chromatin was saved. The leftover samples were precipitated with anti-FLAG antibody which was prebound to Protein G Dynabeads (Thermo Fisher). Cross-linking of the 50 μL of saved chromatin and immunoprecipitated DNA was reversed in a 65°C water bath overnight. After reversal of cross-linking, samples were purified using a Zymo ChIP DNA clean & concentrator (Zymo Research). Five to 10 ng of precipitated DNA was used for library construction using NEBNext ChIP-Seq Library Prep Reagent Set. Sequencing libraries (25 pM) were chemically denatured and applied to an Illumina HiSeq v4 single read flow cell using an Illumina cBot. Hybridized molecules were clonally amplified and annealed to sequencing primers with reagents from an Illumina HiSeq SR Cluster Kit v4-cBot (GD-401–4001). Following transfer of the flow cell to an Illumina HiSeq 2500 instrument (HCSv2.2.38 and RTA v1.18.61), a 50-cycle single-read sequence run was performed using HiSeq SBS Kit v4 sequencing reagents (FC-401–4002). CD3G ChIP-qPCR FWD: CCTCATGAAGAAACGGTCCCA; CD3G ChIP-qPCR RVS: GAGTGCTGGATTCCCACTCA; GFI1 ChIP-qPCR FWD: CCTCTCTCGCCAGTCAATCT; GFI1 ChIP-qPCR RVS: TTGGAGGTCCGGACACTTAG.

ChIP-Seq analysis

SAM (SAM (RRID:SCR_010951) alignments were generated from Illumina Fastq files aligned to the human hg38 genome using Novocraft's novoalign aligner (http://www.novocraft.com) with the following parameters: -o SAM –r Random. Peak calling was then performed using macs2 (https://github.com/taoliu/MACS, v2.1.1.20160309) with the following settings: -g 2.7e9 –call -summit –f BAMPE –nomodel –B –SPMR –extsize 200. Bedgraph files generated were then transformed to bw format using UCSC bedGraphToBigWig application (v4). Heatmap clustering of ChIP-Seq was carried out using deepTools (v3, RRID:SCR_016366). Matrix was generated with computeMatrix application using the following parameters: computeMatrix -S input_1.bw input_2.bw -R peaks.bed–outFileName out.matrix–referencePoint center -a 10000 -b 10000 -bs 100 –sortRegions descend. Correlation heatmap was generated using the deep Tools plot Heatmap application. PCA analysis was performed using the deepTools plotPCA application. The peaks.bed was generated by combining peaks from two ChIP-Seq experiments. plotHeatmap application with default settings was then used to plot heatmap. Peak regions were further used for motif finding analysis, which was carried out using the findMotifGenome.pl application (v4.8.3, HOMER RRID:SCR_010881) with default settings. This resulted in between 92.6M and

Author Manuscript Author Manuscript Author Manuscript Author Manuscript

86.4M reads, wherein between 81.8M and 73.6M (88.3 and 85.2%) uniquely mapped to the Hg38 genome build.

IKZF1 knockout

Nonspecific or *IKZF1*-specific CRISPR/Cas9 RNPs were generated from tracrRNA-ATTO550 (IDT), crRNA (IDT) and Cas9 protein (QB3 MacroLab, UC Berkeley) using commercial guidelines (IDT) and transfected into GFI1–3×FLAG CCRF-CEM cells by electroporation using the Neon transfection system 10 μL kit (ThermoFisher Scientific). Electroporation parameters were 1500V, 10 ms pulse width, 3 pulses. Transfection efficiency was measured by flow cytometry to detect the tracrRNA-ATTO550 positive cells. Approximately 95% transfection efficiency was obtained. Cells were cultured for >9 days to confirm stable ablation of IKAROS protein by Western blotting. CRISPR guide RNAs were chosen targeting the 5' exons of the *IKZF1* gene using the IDT predesigned CRISPR guide RNA database (https://www.idtdna.com/site/order/designtool/index/CRISPR_PREDESIGN). *IKZF1* (PAM site in lower-case): TCATCTGGAGTATCGCTTACagg; GACCTCTCCACCACCTCGGGagg; CTCCAAGAGTGACAGAGTCGtgg. CRISPR/Cas9 negative control crRNA (IDT, 1072544) was used as a control for transfection.

RNA-Seq (Gene Expression Omnibus Series record GSE160183)

Total RNA was extracted from GFI1–3×FLAG CCRF-CEM cells treated with or without doxycycline for 24 hr, and with *IKZF1* or control CRISPR RNP knockout using the RNeasy Mini kit (Qiagen) and RNase-Free DNase Set (Qiagen). RNA integrity numbers (RIN) ranged from 9.4 to 9.9. Poly(A) RNA was purified from total RNA samples (100–500 ng) using oligo(dT) magnetic beads, followed by library construction using the Illumina TruSeq Stranded mRNA Library Prep kit and TruSeq RNA UD Indexes. Purified libraries were qualified on an Agilent Technologies 2200 TapeStation using a D1000 ScreenTape assay. The molarity of adapter-modified molecules was defined by quantitative PCR using the Kapa Biosystems Kapa Library Quant Kit. Individual libraries were normalized to 1.30 nM in preparation for Illumina sequence analysis. NovaSeq 2×50 bp Sequencing_100 M Read-Pairs Sequencing libraries (1.3 nM) were chemically denatured and applied to an Illumina NovaSeq flow cell using the NovaSeq XP chemistry workflow. Following transfer of the flowcell to an Illumina NovaSeq instrument, a 2×51 cycle paired-end sequence run was performed using a NovaSeq S1 reagent Kit.

RNA-Seq analysis

Filtering and alignments were performed using the analysis pipeline developed by the Huntsman Cancer Institute (HCI) Bioinformatic Core Facility (https://huntsmancancerinstitute.github.io/hciRscripts/hciR_scripts.html). Briefly, fastq files were aligned using STAR aligned (v2.7.3a, RRID:SCR_004463) with the following settings: --twopassMode Basic --outSAMtype BAM SortedByCoordinate --limitBAMsortRAM 64000000000 --outBAMsortingBinsN 100 --quantMode TranscriptomeSAM --outWigType bedGraph --outWigStrand Unstranded. The count matrix was then calculated using the Subread FeatureCounts function (v1.6.3) DESeq2 (v1.28.1, RRID:SCR_000154) was used for differentially expressed genes analysis.

Author Manuscript Author Manuscript Author Manuscript Author Manuscript

In vitro SNAG—LSD1 binding assay

Biotinylated, lysine(K)-8 dimethylated SNAG peptide (Bio-K8me2-SNAG) was commercially synthesized and deployed as previously described in CCRF-CEM extracts in either the absence or presence of SP-2509 (19). Biotinylated peptides were collected on streptavidin-Sepharose beads whose non-specific binding sites were blocked in 1% bovine serum albumin (BSA) in 1X phosphate buffered saline (PBS). LSD1 was detected by western blotting in pellets and supernatants.

Data and Reagent Availability Statement

Data presented is available from the corresponding authors. ChIP-Seq and RNA-Seq data sets are available through the Gene Expression Omnibus (GEO) portal via series record GEO160183). Proteomics data is accessible in MassIVE via the file identifier, MSV000086405. All expression constructs and renewable reagents are available to the scientific community upon request.

Results

GFI1 proximitome proteomics in T-ALL cells

To identify potential GFI1 cooperating proteins in T-ALL, we applied the BioID (Biotin IDentification) proximity-dependent labeling method (Figure 1A). We generated doxycycline-inducible, GFI1-BirA*-expressing CCRF-CEM cells. GFI1-BirA* protein expression was comparable to that of endogenously expressed GFI1 (Supplementary Figure S1A). In parallel, cells transduced with empty vector or BirA* only were generated as controls, and BirA* protein expression was equivalent to that of GFI1-BirA* (Figure 1B). Cells were incubated in biotin-containing medium, treated with doxycycline and lysates prepared. Biotinylated proteins were collected with streptavidin (SAv)-Sepharose beads and surveyed for known GFI1 interacting partners (Figure 1C). As expected, we detected comparable biotinylation of GFI1-BirA* and BirA*, suggesting the presence of GFI1 protein structure in the fusion protein does not interfere with the formation of reactive biotin-AMP by BirA*. Moreover, we find an altered pattern of biotinylated proteins when BirA* activity is tethered to GFI1, and enrichment for known GFI1 interacting partners, LSD1 and CoREST among biotinylated proteins in cells expressing GFI1-BirA* vs. BirA* control. These data validate the technique for detecting GFI1 proximity partners proteome-wide.

To identify the complete cohort of GFI1 proximity partners, biotinylated proteins were purified on streptavidin (SAv)-Sepharose beads and subjected to unbiased, proteome-wide LC-MS/MS (Figure 1A). Three replicates were performed for each condition (Vector, BirA* and GFI1-BirA*). A total of 502 interacting proteins were identified that demonstrated both increased mass spectrometry intensity in the presence of doxycycline compared to empty vector control and a BirA* vs GFI1- BirA* *P*-value <0.05 (Supplemental Table S1). Proximity partners were analyzed as previously described (20). A volcano plot showing fold change in average sum read intensities ($\log_2$ (GFI1-WT/BirA*)) relative to *P*-value ($-\log_{10}$ *P*-value) is shown in Figure 2A. Being covalently tethered to BirA*, the placement of GFI1 in the top right corner of the plot is an important quality control, signifying the most

Author Manuscript Author Manuscript Author Manuscript Author Manuscript

statistically significant *P*-value and most abundantly enriched protein in the data set. Among biotinylated proteins, known GFI1 partners LSD1 (KDM1A), CoREST (RCOR1), STAG1, BCL11A and HMG20B were enriched when comparing GFI1-BirA* to BirA* only (Figure 2A, shown in red). Among newly-identified GFI1 proximity partners, the strongest overall by fold-enrichment was for IKZF1/IKAROS (Figure 2A). To identify possible functional protein associations, we clustered the top 40 GFI1-proximate proteins using the STRING functional protein—protein association network (21). The majority of these proteins were annotated as being nuclear and involved in regulating gene expression (Figure 2B, red and blue circles respectively). Notably, STRING output linked GFI1 directly to LSD1 and CoREST, as expected (Figure 2B), but placed IKAROS more remotely, arguing against a direct interaction with GFI1 (Figure 2B).

The GFI1—IKAROS interaction requires intact GFI1 and IKAROS DNA binding

We validated the proximity relationship between IKAROS and GFI1 through Western blotting. First, we tested if N-terminal GFI1 mutations known to block binding to LSD1 also block the ability to transfer biotin moieties to IKAROS. GFI1 mutations that block LSD1 binding did not affect IKAROS proximity labeling (Figure 3A). Additionally, GFI1 and IKAROS failed to interact using a variety of traditional co-immunoprecipitation conditions (Figure 3B). One possible explanation for the discrepancy could be that GFI1 and IKAROS co-occupy nearby DNA binding sites at common target genes such that their proximity enables biotin moieties to be frequently transferred from GFI1-BirA* to IKAROS even though the two proteins do not interact directly in solution. Similarly, GFI1 and IKAROS could occupy sites distant from one another but be brought together through interactions involving a shared protein complex. These models predict that the proximity relationship between GFI1 and IKAROS would require both proteins to bind DNA, and that a defect in DNA binding by either protein would attenuate the proximity relationship between them. Previous work on GFI1 and IKAROS has identified specific domains and mutants that control DNA binding activity (22,23). We established these DNA-binding deficient mutations in GFI1 (N383S in rat GFI1, which corresponds to N382S in human GFI1) and IKAROS (N159A) and used them to interrogate the GFI1—IKAROS proximity relationship. GFI1-N383S-BirA* reduced proximity labeling of wild type IKAROS (Figure 3C). Likewise, we observed a comparable reduction in proximity labeling of IKAROS-N159A when tested with wild type GFI1-BirA*. When both DNA-binding deficient mutants were combined, the proximity relationship between GFI1 and IKAROS was abolished (Figure 3C). These results indicate that the proximity relationship between GFI1 and IKAROS relies upon their shared ability to bind DNA and suggests a mechanism for GFI1 and IKAROS to cooperate to control a common set of genes through near or distant regulatory regions.

GFI1 and IKAROS associate with common genes, including genes associated with T cell development

To further study the interplay between GFI1 and IKAROS, we conducted ChIP-Seq using CCRF-CEM cells expressing 3×FLAG-tagged GFI1 or IKAROS (GFI1–3×FLAG or IKAROS-3×FLAG) under doxycycline-inducible control. FLAG immunoblotting confirmed inducible and comparable expression of the two proteins (Figure 4A). Two replicates each

Author Manuscript Author Manuscript Author Manuscript Author Manuscript

for GFI1 and IKAROS ChIP were performed. Sequencing of the ChIP material resulted in 25,674 total GFI1 and 52,759 IKAROS peaks. The signals from input, GFI1 ChIP-Seq and IKAROS ChIP-Seq replicates were highly correlated, with Spearman correlation R-values >0.8. Further, the GFI1 and IKAROS ChIP-Seq signals were highly correlated, with R values >0.75. (Supplementary Figure S1B). Principal component analysis of the bound peaks also indicated the inputs and ChIP replicates from the two cells lines were more similar to each other compared to other samples (Supplementary Figure S1C). Approximately 80% of GFI1-bound peaks overlap (at least one bp) with peaks bound by IKAROS (Figure 4B), suggesting that they regulate common targets. To investigate this more closely, we centered binding peaks from either or both ChIP experiments (57,841 peaks) by peak summit, and arranged them as a heatmap from strongest to weakest GFI1 binding (Figure 4C, left side) and IKAROS binding (Figure 4C, right side). The mean distance between peak summits for GFI1- and IKAROS-bound loci was 136bp and the median distance was 98bp. These results indicate a strong overall correlation between GFI1 and IKAROS binding across the genome. Motif analysis using all identified peaks showed that GFI1 and IKAROS shared four of the top five most significant binding motifs (Supplementary Figure S1D), again suggesting common gene binding. Among the top shared motifs is FLI1, an Ets transcription factor (consensus TTCC or GGAA reverse complement). Out of the top 20 enriched motifs for the two datasets, 14 and 15 Ets transcription motifs were present (Supplementary Figure S1D). IKAROS is known to interact with Ets motifs (24).

GFI1 and IKAROS play crucial roles in hematopoiesis, including in T cells (25–27). Consistently, gene ontology (GO) analysis of genes within 6 kb of the GFI1- and IKAROS-bound peaks (using GREAT v4.0.4) identifies hematopoiesis and TCR recombination as common terms (Supplemental Table S2). Example bound targets are shown in Figure 4D, including genes encoding key transcription factors required for T cell development such as *GFI1* itself, *MYC*, *MYB*, *HES1, RUNX3* and *TCF3*. Other examples include *NOTCH3* and genes in the *CD3* cluster. Figure 4D also shows previously published RNA-Seq data (28) indicating that these genes are all expressed in CCRF-CEM cells.

GFI1 and IKAROS positively regulate a subset of target genes

We used bulk RNA-Seq with GFI1–3×FLAG CCRF-CEM cells to identify changes in gene expression associated with either ectopic GFI1 expression or CRISPR-mediated *IKZF1* knockout leading to IKAROS depletion. For knockouts, we transfected GFI1–3×FLAG cells with CRISPR RNPs containing Cas9 protein, fluorescently-conjugated tracrRNA and either a nonspecific or *IKZF1*-specific sgRNA. Successfully transfected cells were sorted on the following day and cultured for an additional 9 days before treatment with doxycycline or vehicle for 24 hrs (see methods). This resulted in robust knockout using specific but not control RNPs (Figure 5A). A similar knockout strategy targeting *GFI1* resulted in lethality in CCRF-CEM cells, consistent with prior studies (19) and underscoring its critical pro-survival role. For this reason studies with *GFI1* knockout in CCRF-CEM cells were not pursued further. Three independent replicates were performed for each of the four conditions, with the exception of vehicle-treated IKAROS knockout with two replicates. Between 21.7 and 28.2 million RNA-Seq reads were generated for each

Author Manuscript Author Manuscript Author Manuscript Author Manuscript

condition, wherein 88.6 to 90.3% of these aligned uniquely to the human *Hg38* reference genome. Approximately 99% of the reads within coding regions aligned to the correct strand (Supplemental Table S3). Hierarchical clustering of the top 500 most significantly differentially regulated genes across all the conditions (ranked based on *P*-value) revealed groups of genes repressed and activated by the different conditions. For example, a large number of genes were de-repressed with IKAROS knockout and/or repressed with GFI1 overexpression (Figure 5B, clusters 1, 2, 3). Another group, not strongly affected by GFI1, was repressed with IKAROS knockout (cluster 5). However, a small group of 38 genes (cluster 4) were induced by GFI1 overexpression (Figure 5B). This same group of genes was also repressed with IKAROS knockout. Interestingly, when ectopic GFI1 expression and IKAROS knockout were combined, the induction of these genes was significantly blunted, suggesting IKAROS is required for GFI1-mediated transactivation (Figure 5B). These genes include *RAG1*, the *CD3* cluster and *NOTCH3* (Supplemental Table S4). Intersecting this set of positively regulated genes with the ChIP-Seq data reveals that 68.4% (26 of 38 total genes in cluster 4) have GFI1 and IKAROS peaks located <10 kb from their transcription start sites, strongly suggesting they are direct targets of both GFI1 and IKAROS (Supplemental Table S4). 34.2% of these genes (13/38) show promoter binding (<500 bp from TSS) of both proteins. RNA-Seq genome tracks for *NOTCH3* are shown in Figure 5C alongside the GFI1 and IKAROS ChIP-Seq reads. Strong and overlapping GFI1 and IKAROS peaks are present in the 5' region of the gene. Examining the genomic sequence of the *NOTCH3* gene for putative GFI1 and IKAROS binding sites reveals a single GFI1 consensus site [TAAATCAC(A/T)GCA] and six potential IKAROS consensus sites [(A/G)GGAAG or CTTCC(T/C)] within its first intron (*hg19* chr19: 15308391–15309391). In the RNA-Seq, *NOTCH3* is induced by ectopic GFI1 expression and inhibited by IKAROS knockout, while the combination significantly blunts induction by GFI1. No such changes were observed for *NOTCH1* or *NOTCH2*, which show some GFI1 and IKAROS association but constitutive expression, or for *NOTCH4*, which shows no binding and is not expressed in CCRF-CEM cells (Supplementary Figure S2).

GFI1 and IKAROS cooperatively regulate NOTCH3

A model in which GFI1 and IKAROS interact on DNA to induce the expression of specific genes predicts that overexpression of either protein should induce target gene expression. Both GFI1 and IKAROS interact with the *NOTCH3* gene. In addition, NOTCH3 activating mutations can trigger T-ALL development (16–18). For these reasons, and because its surface expression can easily be measured using flow cytometry, we used *NOTCH3* as an example target gene. We treated CCRF-CEM cells that inducibly express GFI1–3×FLAG with doxycycline and followed surface NOTCH3 expression as a time course. NOTCH3 was low but detectable in untreated cells (Figure 6A, 0h), with expression increasing during the 48 hour treatment course. Expression increased as measured by the percentage of positive cells and by mean fluorescence intensity (MFI). CCRF-CEM cells inducibly expressing IKAROS-3×FLAG were similarly able to increase NOTCH3 cell surface expression (Figure 6B).

We then replaced the GFI1 lentiviral construct with a truncation mutant in which the SNAG domain was deleted (ΔSNAG) or with a SNAG domain point mutant that no longer interacts

Author Manuscript Author Manuscript Author Manuscript Author Manuscript

with LSD1 to mediate transcriptional repression (P2A) (19,29). Unexpectedly, these mutant forms of GFI1 no longer augment surface NOTCH3 expression (Figure 6C). These results suggest that GFI1 and IKAROS collaborate to transactivate the *NOTCH3* gene, and that GFI1 does so, at least in part, though residues that are also important to recruit LSD1. To more directly determine the role of LSD1 in GFI1-mediated NOTCH3 induction in CCRF-CEM cells, we utilized the non-competitive LSD1 inhibitor, SP-2509 (30,31). Surprisingly, NOTCH3 expression significantly increased in cells treated with SP-2509 compared to DMSO vehicle control even without doxycycline treatment (Figure 6D). Doxycycline-induced GFI1 expression cooperated with SP-2509 to further increase NOTCH3 expression at 24 but not 48 hr (Figure 6D). We obtained similar results for NOTCH3 cell surface expression using SUP-T1 (Figure 7A) and Jurkat (Supplementary Figure S3E) T-ALL cell lines, where doxycycline-induced GFI1 expression or LSD1 inhibition with SP-2509 elevated surface levels of NOTCH3. We then explored *CD3* as a second target regulated by the GFI1—IKAROS partnership. We confirmed co-occupancy by GFI1 and IKAROS on the *CD3G* promoter using ChIP-qPCR (Supplementary Figure S4A) and then demonstrated increased CD3 cell surface expression from enforced expression of GFI1 in both CCRF-CEM and SUP-T1 cells (Supplementary Figure S4B and S4C). CD3 expression also increased with IKAROS overexpression in CCRF-CEM cells (Supplementary Figure S4D) and decreased with either lenalidomide treatment or IKAROS knockout (Supplementary Figure S5).

Notably, results obtained using SNAG domain mutants (ΔSNAG and P2A) are the reverse of those obtained with SP-2509, where the SNAG domain remains intact. We hypothesized this positive impact of SP-2509 could represent targeted disruption of the interaction between LSD1 and the SNAG domain to enable alternative interactions involving candidate co-activators. Small molecule inhibitors of LSD1 can disrupt binding between GFI1 and LSD1(32). Further, we have previously shown the SNAG domain is sufficient for LSD1 binding and that dimethyl modification at lysine 8 (K8me2) of the SNAG domain strongly favors LSD1binding in an *in vitro* binding assay. We deployed this assay (Figure 7B, left panel) to test the impact of SP-2509 on SNAG—LSD1 binding. SP-2509 abolished binding between LSD1 and a biotinylated K8me2-SNAG peptide (Figure 7B, right panel). These results suggest the SNAG—LSD1 interaction can be modulated to enable competition between LSD1 and one or more unknown proteins for SNAG domain binding and regulation of GFI1-mediated transcriptional output.

We then tested the effect of IKAROS depletion on GFI1-induced NOTCH3 expression using GFI1–3×FLAG CCRF-CEM cells. Lenalidomide is well-documented to rapidly and efficiently trigger degradation of IKAROS (33). Induction of cell surface NOTCH3 expression was significantly impaired by Lenalidomide treatment compared with DMSO control (Figure 7C). Immunoblotting confirmed the rapid loss of IKAROS protein and unaltered expression of ectopic GFI1 in the presence of Lenalidomide (Supplementary Figure S3A–B). We obtained similar results using cells electroporated with *IKZF1*-targeted CRISPR RNPs (Figure 7D, Supp. Figure 3C–D). These results strongly suggest that IKAROS and GFI1 act in a cooperative fashion to transactivate a specific subset of genes which includes *NOTCH3*, and given the tumor promoting role of constitutively active NOTCH3 could provide a new direction for therapeutic development in T-ALL (Figure 7E).

Author Manuscript Author Manuscript Author Manuscript Author Manuscript

Discussion

Identifying the molecular determinants of T cell development furthers understanding of T-ALL pathogenesis. The zinc finger transcription factor GFI1 plays critical roles in myeloid and lymphoid development and is an important pro-survival factor in T-ALL (10). The protein partnerships on which GFI1 depends for this role may offer potential therapeutic targets in T-ALL, but are as yet ill-defined. Here, using an unbiased quantitative proximity labeling approach, we identify GFI1 interacting proteins in T-ALL cells. Among these, IKAROS serves as a cooperating partner for GFI1-mediated gene regulation. Functional studies using T-ALL cells reveal a previously unrecognized role for GFI1 in transcriptional activation of genes that are among its targets, and several of which are involved in T cell development.

GFI1 and its paralog, GFI1B, have been largely described as a transcriptional repressors, and indeed can partially substitute for one another *in vivo*. Repression requires a highly conserved 20-amino acid N-terminal SNAG domain capable of recruiting LSD1 complexed with CoREST (34). In previous studies, point mutations or truncations in the SNAG domain that disrupt GFI1/1B—LSD1 binding impair GFI1/1B functions in multiple assays, pinpointing LSD1 as a central cofactor in GFI1/1B-mediated transcriptional repression and the establishment of downstream phenotypes (19,20,29,34). However, it is not clear whether GFI1/1B can regulate gene expression through other mechanisms, especially in cooperation with other factors. We applied BioID proximity labeling to identify GFI1-interacting proteins, where a promiscuous biotin ligase (BirA*) (35) is fused to GFI1. Relative to co-immunoprecipitation, this method has the advantage that transient and indirect interactions can be efficiently captured. We utilized this method together with human CCRF-CEM T-ALL cells to systematically label proteins spatially close to GFI1, identifying GFI1 itself and some 500 direct or indirect interacting partners. Among these are previously identified GFI1-interacting proteins HMG20B, STAG1 and components of the BHC complex including LSD1, CoREST, and GSE1. We segregated interacting proteins into functional groups and analyzed their network relationships. Through this analysis we identified IKAROS, encoded by the *IKZF1* gene, as a top hit. IKAROS is also a zinc finger transcription factor that plays multiple, key roles in hematopoiesis, including in the development of B and T cells (27,36,37). As with GFI1, IKAROS has also been linked to mouse and human T-ALL. In T-ALL, IKAROS functions as a tumor suppressor, and its deletion is a poor prognostic indicator for affected patients (38,39). This impact on prognosis takes on a new dimension when considered in the context of the GFI1—IKAROS partnership.

GFI1 and IKAROS do not co-precipitate in conventional co-IP assays, suggesting their interaction is indirect and transient in nature. Biotin transfer between the two proteins depends on DNA binding but does not depend on the GFI1 SNAG domain. Because GFI1 and IKAROS are both sequence-specific DNA binding proteins, we performed ChIP-Seq to identify potential common target genes. This effort identified >25,000 GFI1-bound and >50,000 IKAROS-bound peaks. The large number of IKAROS peaks is consistent with previous reports for IKAROS binding in human K562 and myeloma cell lines (40,41) and may be attributable to its ability to bind DNA in multimeric configurations (42).

Author Manuscript Author Manuscript Author Manuscript Author Manuscript

Approximately 80% (19966/25674) of GFI1 bound peaks overlap with IKAROS peaks, supporting the idea that the two proteins frequently co-regulate target gene expression. Co-occupied targets include *GFI1* itself, as well as *NOTCH3*, the *CD3* gene cluster (*CD3E*, *CD3D* and *CD3G*), *TCF3*, *MYC*, *RUNX3*, *MYB* and *HES1*, each with fundamental roles in T-cell development. Interplay between GFI1 and other transcription factors has been described. For example, GFI1 and HOXA9 compete for overlapping binding sites at a distinct class of targets in AML (43). Unlike HOXA9, our results suggest that IKAROS cooperates with GFI1.

RNA-Seq gene expression profiling using CCRF-CEM cells with ectopic GFI1 expression and/or with IKAROS knockout revealed a group of genes positively regulated by both proteins. Among these genes are *NOTCH3, CD3* and *RAG1*, while other NOTCH family members *NOTCH1*, *NOTCH2*, and *NOTCH4* were not affected by enforced expression of GFI1. This indicates *NOTCH3* is the specific NOTCH gene targeted for induction by the GFI1—IKAROS partnership. This is reinforced by the finding of GFI1 and IKAROS consensus sites within the first intron of the *NOTCH3* gene. Moreover, genes making up this group are enriched for GFI1 and IKAROS occupancy, strongly suggesting they are direct targets and that the positive effects of the GFI1—IKAROS partnership on transcription are also direct in nature. Yet, confirmation of this model will depend upon first identifying and then specifically disrupting GFI1 and IKAROS binding sites in coregulated genes like *NOTCH3*. This uncertainty is a limitation of our study.

In CCRF-CEM cells a *NOTCH1*-activating mutation and *FBXW7* loss-of-function drive constitutive NOTCH signaling (44). Similarly, SUP-T1 cells carry a t(7;9) translocation driving expression of a truncated NOTCH variant to produce constitutive, ligand-independent NOTCH activity (45). Using both cell lines, we find that GFI1 and IKAROS promote NOTCH3 cell surface expression. Moreover, mutations in the GFI1 SNAG domain that block the interaction with LSD1 also render GFI1 incapable of inducing NOTCH3. It is not clear whether LSD1 itself is important for this activation (e.g., through demethylating repressive protein modifications such as H3K9 methylation), or whether interactions between the SNAG domain and some other positively-acting cofactor become dominant in the case of GFI1—IKAROS coregulated genes. Interestingly, SP-2509 and SNAG mutants, both of which disrupt GFI1—LSD1 binding, yield opposite results in NOTCH3 cell surface expression. Because SP-2509 leaves SNAG domain primary structure intact, our findings could indicate that LSD1 and an as yet unidentified co-activator compete for SNAG domain binding in an IKAROS-dependent manner. To address this possibility, we used lenalidomide to acutely degrade IKAROS protein. Lenalidomide is a thalidomide derivative that is active in multiple myeloma by enabling targeted degradation of IKAROS (33). We find that acute IKAROS depletion blunts GFI1-mediated transactivation and cell surface expression of NOTCH3, consistent with GFI1 and IKAROS providing a platform for SNAG-dependent recruitment of a transcriptional co-activating principle, leading to transactivation of a gene expression program represented by the *NOTCH3* response. It is notable that in multiple T-ALL cell lines GFI1 loss is lethal while IKAROS depletion is tolerated. These observations suggest that GFI1—IKAROS coregulated genes alone are not required for cell survival, and instead fulfill other functions in T-ALL homeostasis. It may also indicate functional redundancy for IKAROS family proteins but not for GFI1, or

Author Manuscript Author Manuscript Author Manuscript Author Manuscript

perhaps that GFI1-regulated genes critical for cell survival are independent of IKAROS. Equally notable is that despite their distinct phenotypic contributions, there is substantial overlap between GFI1 and IKAROS binding sites across the genome, while only a subset of genes show significantly altered expression because of their partnership. This finding suggests that concurrent transcription factor binding may overestimate functionally relevant partnerships and imply that co-occupancy may not always be consequential or may have impacts that are not easily measured. We posit that the significance of shared occupancy is magnified when it correlates with changes in gene expression, and that this may occur for only a small subset of co-occupied loci.

Cumulatively, the results support a model in which the presence of IKAROS allows for activation of target genes by GFI1 (Figure 7E). This model is consistent with the identification of SWI/SNF, a chromatin remodeling complex associated with positive regulation of gene expression (46,47), as a GFI1 proximity partner. Transactivating potential for both IKAROS and GFI1 has been described previously. IKAROS binds and activates *Cd3d* through an upstream enhancer region (27,36). CD3 proteins form a central component of the T cell receptor signaling complex. Positive regulation of gene expression by GFI1 was found in mouse granulocyte-monocyte precursor cells (GMPs) undergoing a binary monocyte/granulocyte fate decision. In GMPs it was shown that GFI1 associates with granulocyte-specific targets such as *Per3* and *Ets1*, activating their expression as part of a broader granulocyte fate-specifying program. Concurrently, GFI1 binding and repression of monocyte-specific genes suppresses the monocyte program (48). It seems reasonable to posit that concurrent activation and repression of opposing gene expression programs, such as those exemplified by the GFI1—IKAROS—LSD1 relationship, could direct alternative outcomes in developmental hematopoiesis and that disruptions in these relationships could be permissive for malignancy. More work is necessary to define the molecular mechanisms by which GFI1 switches between repressive and activating transcriptional potential to control these binary fate decisions.

Supplementary Material

Refer to Web version on PubMed Central for supplementary material.

Acknowledgements

This work was supported by a National Institutes of Health Cancer Center Support Grant [P30CA042014], National Institutes of Health grants [R01CA201235] to M Engel, [R01GM122778, R01AI100873] to D Tantin and grants to M Engel from American Cancer Society and Alex's Lemonade Stand Foundation.

We thank F. Gounari and P. Ernst for critical reading of the manuscript. DNA sequencing and DNA oligonucleotides were synthesized by the University of Utah Health Sciences Center DNA/Peptide Synthesis Facility. We thank R. Tomaino at Taplin Mass Spectrometry Facility, Cell Biology Department, Harvard Medical School for assistance with LS-MS/MS and analysis. ChIP-Seq and RNA-Seq data reported in this study utilized the University of Utah Huntsman Cancer Institute High-Throughput Genomics and Bioinformatic Analysis Shared Resources. We thank C. Stubben at the Huntsman Cancer Institute Bioinformatics Shared Resource for assistance with submitting NGS sequencing data to GEO, and S.M. Osburn at the University Mass Spectrometry Facility for assistance with submitting mass spectrometry data to MassIVE.

Additional information

Author Manuscript Author Manuscript Author Manuscript Author Manuscript

Financial support:

This work was supported by a National Institutes of Health Cancer Center Support Grant [P30CA042014], National Institutes of Health grants [R01CA201235] to MEE, [R01GM122778, R01AI100873] to DT and grants to MEE from American Cancer Society and Alex's Lemonade Stand Foundation

References

1. Zeng H, Yucel R, Kosan C, Klein-Hitpass L, Moroy T. Transcription factor Gfi1 regulates self-renewal and engraftment of hematopoietic stem cells. EMBO J 2004;23(20):4116–25 doi 10.1038/sj.emboj.7600419. [PubMed: 15385956]
2. Hock H, Hamblen MJ, Rooke HM, Schindler JW, Saleque S, Fujiwara Y, et al. Gfi-1 restricts proliferation and preserves functional integrity of haematopoietic stem cells. Nature 2004;431(7011):1002–7 doi 10.1038/nature02994. [PubMed: 15457180]
3. Person RE, Li FQ, Duan Z, Benson KF, Wechsler J, Papadaki HA, et al. Mutations in proto-oncogene GFI1 cause human neutropenia and target ELA2. Nat Genet 2003;34(3):308–12 doi 10.1038/ng1170. [PubMed: 12778173]
4. Hock H, Hamblen MJ, Rooke HM, Traver D, Bronson RT, Cameron S, et al. Intrinsic requirement for zinc finger transcription factor Gfi-1 in neutrophil differentiation. Immunity 2003;18(1):109–20. [PubMed: 12530980]
5. Karsunky H, Zeng H, Schmidt T, Zevnik B, Kluge R, Schmid KW, et al. Inflammatory reactions and severe neutropenia in mice lacking the transcriptional repressor Gfi1. Nat Genet 2002;30(3):295–300 doi 10.1038/ng831. [PubMed: 11810106]
6. Yucel R, Karsunky H, Klein-Hitpass L, Moroy T. The transcriptional repressor Gfi1 affects development of early, uncommitted c-Kit+ T cell progenitors and CD4/CD8 lineage decision in the thymus. J Exp Med 2003;197(7):831–44 doi 10.1084/jem.20021417. [PubMed: 12682108]
7. Volpe G, Walton DS, Grainger DE, Ward C, Cauchy P, Blakemore D, et al. Prognostic significance of high GFI1 expression in AML of normal karyotype and its association with a FLT3-ITD signature. Sci Rep 2017;7(1):11148 doi 10.1038/s41598-017-11718-8. [PubMed: 28894287]
8. Hones JM, Botezatu L, Helness A, Vadnais C, Vassen L, Robert F, et al. GFI1 as a novel prognostic and therapeutic factor for AML/MDS. Leukemia 2016;30(6):1237–45 doi 10.1038/leu.2016.11. [PubMed: 26847026]
9. Khandanpour C, Krongold J, Schutte J, Bouwman F, Vassen L, Gaudreau MC, et al. The human GFI136N variant induces epigenetic changes at the Hoxa9 locus and accelerates K-RAS driven myeloproliferative disorder in mice. Blood 2012;120(19):4006–17 doi 10.1182/blood-2011-02-334722. [PubMed: 22932805]
10. Khandanpour C, Phelan JD, Vassen L, Schutte J, Chen R, Horman SR, et al. Growth factor independence 1 antagonizes a p53-induced DNA damage response pathway in lymphoblastic leukemia. Cancer Cell 2013;23(2):200–14 doi 10.1016/j.ccr.2013.01.011. [PubMed: 23410974]
11. Zhang J, Ding L, Holmfeldt L, Wu G, Heatley SL, Payne-Turner D, et al. The genetic basis of early T-cell precursor acute lymphoblastic leukaemia. Nature 2012;481(7380):157–63 doi 10.1038/nature10725. [PubMed: 22237106]
12. Terwilliger T, Abdul-Hay M. Acute lymphoblastic leukemia: a comprehensive review and 2017 update. Blood Cancer J 2017;7(6):e577 doi 10.1038/bcj.2017.53. [PubMed: 28665419]
13. Golde TE, Koo EH, Felsenstein KM, Osborne BA, Miele L. gamma-Secretase inhibitors and modulators. Biochim Biophys Acta 2013;1828(12):2898–907 doi 10.1016/j.bbamem.2013.06.005. [PubMed: 23791707]
14. Bellavia D, Campese AF, Alesse E, Vacca A, Felli MP, Balestri A, et al. Constitutive activation of NF-kappaB and T-cell leukemia/lymphoma in Notch3 transgenic mice. EMBO J 2000;19(13):3337–48 doi 10.1093/emboj/19.13.3337. [PubMed: 10880446]
15. Waegemans E, Van de Walle I, De Medts J, De Smedt M, Kerre T, Vandekerckhove B, et al. Notch3 activation is sufficient but not required for inducing human T-lineage specification. J Immunol 2014;193(12):5997–6004 doi 10.4049/jimmunol.1400764. [PubMed: 25381438]
16. Bernasconi-Elias P, Hu T, Jenkins D, Firestone B, Gans S, Kurth E, et al. Characterization of activating mutations of NOTCH3 in T-cell acute lymphoblastic leukemia and anti-leukemic

Author Manuscript Author Manuscript Author Manuscript Author Manuscript

activity of NOTCH3 inhibitory antibodies. Oncogene 2016;35(47):6077–86 doi 10.1038/onc.2016.133. [PubMed: 27157619]

17. Choi SH, Severson E, Pear WS, Liu XS, Aster JC, Blacklow SC. The common oncogenomic program of NOTCH1 and NOTCH3 signaling in T-cell acute lymphoblastic leukemia. PLoS One 2017;12(10):e0185762 doi 10.1371/journal.pone.0185762. [PubMed: 29023469]
18. Tottone L, Zhdanovskaya N, Carmona Pestana A, Zampieri M, Simeoni F, Lazzari S, et al. Histone Modifications Drive Aberrant Notch3 Expression/Activity and Growth in T-ALL. Front Oncol 2019;9:198 doi 10.3389/fonc.2019.00198. [PubMed: 31001470]
19. Velinder M, Singer J, Bareyan D, Meznarich J, Tracy CM, Fulcher JM, et al. GFI1 functions in transcriptional control and cell fate determination require SNAG domain methylation to recruit LSD1. Biochem J 2017;474(17):2951 doi 10.1042/BCJ-2016-0558_COR. [PubMed: 28801480]
20. McClellan D, Casey MJ, Bareyan D, Lucente H, Ours C, Velinder M, et al. Growth Factor Independence 1B-Mediated Transcriptional Repression and Lineage Allocation Require Lysine-Specific Demethylase 1-Dependent Recruitment of the BHC Complex. Mol Cell Biol 2019;39(13) doi 10.1128/MCB.00020-19.
21. Szklarczyk D, Gable AL, Lyon D, Junge A, Wyder S, Huerta-Cepas J, et al. STRING v11: protein-protein association networks with increased coverage, supporting functional discovery in genome-wide experimental datasets. Nucleic Acids Res 2019;47(D1):D607–D13 doi 10.1093/nar/gky1131. [PubMed: 30476243]
22. Zarebski A, Velu CS, Baktula AM, Bourdeau T, Horman SR, Basu S, et al. Mutations in growth factor independent-1 associated with human neutropenia block murine granulopoiesis through colony stimulating factor-1. Immunity 2008;28(3):370–80 doi 10.1016/j.immuni.2007.12.020. [PubMed: 18328744]
23. Kuehn HS, Boisson B, Cunningham-Rundles C, Reichenbach J, Stray-Pedersen A, Gelfand EW, et al. Loss of B Cells in Patients with Heterozygous Mutations in IKAROS. N Engl J Med 2016;374(11):1032–43 doi 10.1056/NEJMoa1512234. [PubMed: 26981933]
24. Zhang J, Jackson AF, Naito T, Dose M, Seavitt J, Liu F, et al. Harnessing of the nucleosome-remodeling-deacetylase complex controls lymphocyte development and prevents leukemogenesis. Nat Immunol 2011;13(1):86–94 doi 10.1038/ni.2150. [PubMed: 22080921]
25. Shi LZ, Kalupahana NS, Turnis ME, Neale G, Hock H, Vignali DA, et al. Inhibitory role of the transcription repressor Gfi1 in the generation of thymus-derived regulatory T cells. Proc Natl Acad Sci U S A 2013;110(34):E3198–205 doi 10.1073/pnas.1300950110. [PubMed: 23918371]
26. Tinsley KW, Hong C, Luckey MA, Park JY, Kim GY, Yoon HW, et al. Ikaros is required to survive positive selection and to maintain clonal diversity during T-cell development in the thymus. Blood 2013;122(14):2358–68 doi 10.1182/blood-2012-12-472076. [PubMed: 23908463]
27. Georgopoulos K, Bigby M, Wang JH, Molnar A, Wu P, Winandy S, et al. The Ikaros gene is required for the development of all lymphoid lineages. Cell 1994;79(1):143–56 doi 10.1016/0092-8674(94)90407-3. [PubMed: 7923373]
28. Quentmeier H, Pommerenke C, Dirks WG, Eberth S, Koeppel M, MacLeod RAF, et al. The LL-100 panel: 100 cell lines for blood cancer studies. Sci Rep 2019;9(1):8218 doi 10.1038/s41598-019-44491-x. [PubMed: 31160637]
29. Grimes HL, Chan TO, Zweidler-McKay PA, Tong B, Tsichlis PN. The Gfi-1 proto-oncoprotein contains a novel transcriptional repressor domain, SNAG, and inhibits G1 arrest induced by interleukin-2 withdrawal. Mol Cell Biol 1996;16(11):6263–72 doi 10.1128/mcb.16.11.6263. [PubMed: 8887656]
30. Fiskus W, Sharma S, Shah B, Portier BP, Devaraj SGT, Liu K, et al. Highly effective combination of LSD1 (KDM1A) antagonist and pan-histone deacetylase inhibitor against human AML cells. Leukemia 2017;31(7):1658 doi 10.1038/leu.2017.77. [PubMed: 28322226]
31. Inui K, Zhao Z, Yuan J, Jayaprakash S, Le LTM, Drakulic S, et al. Stepwise assembly of functional C-terminal REST/NRSF transcriptional repressor complexes as a drug target. Protein Sci 2017;26(5):997–1011 doi 10.1002/pro.3142. [PubMed: 28218430]
32. Maiques-Diaz A, Spencer GJ, Lynch JT, Ciceri F, Williams EL, Amaral FMR, et al. Enhancer Activation by Pharmacologic Displacement of LSD1 from GFI1 Induces Differentiation in Acute

Author Manuscript Author Manuscript Author Manuscript Author Manuscript

Myeloid Leukemia. Cell Rep 2018;22(13):3641–59 doi 10.1016/j.celrep.2018.03.012. [PubMed: 29590629]

33. Lu G, Middleton RE, Sun H, Naniong M, Ott CJ, Mitsiades CS, et al. The myeloma drug lenalidomide promotes the cereblon-dependent destruction of Ikaros proteins. Science 2014;343(6168):305–9 doi 10.1126/science.1244917. [PubMed: 24292623]
34. Saleque S, Kim J, Rooke HM, Orkin SH. Epigenetic regulation of hematopoietic differentiation by Gfi-1 and Gfi-1b is mediated by the cofactors CoREST and LSD1. Mol Cell 2007;27(4):562–72 doi 10.1016/j.molcel.2007.06.039. [PubMed: 17707228]
35. Kim DI, Jensen SC, Noble KA, Kc B, Roux KH, Motamedchaboki K, et al. An improved smaller biotin ligase for BioID proximity labeling. Mol Biol Cell 2016;27(8):1188–96 doi 10.1091/mbc.E15-12-0844. [PubMed: 26912792]
36. Georgopoulos K, Moore DD, Derfler B. Ikaros, an early lymphoid-specific transcription factor and a putative mediator for T cell commitment. Science 1992;258(5083):808–12. [PubMed: 1439790]
37. Hahm K, Ernst P, Lo K, Kim GS, Turck C, Smale ST. The lymphoid transcription factor LyF-1 is encoded by specific, alternatively spliced mRNAs derived from the Ikaros gene. Mol Cell Biol 1994;14(11):7111–23 doi 10.1128/mcb.14.11.7111. [PubMed: 7935426]
38. Winandy S, Wu P, Georgopoulos K. A dominant mutation in the Ikaros gene leads to rapid development of leukemia and lymphoma. Cell 1995;83(2):289–99 doi 10.1016/0092-8674(95)90170-1. [PubMed: 7585946]
39. Marcais A, Jeannet R, Hernandez L, Soulier J, Sigaux F, Chan S, et al. Genetic inactivation of Ikaros is a rare event in human T-ALL. Leuk Res 2010;34(4):426–9 doi 10.1016/j.leukres.2009.09.012. [PubMed: 19796813]
40. Barwick BG, Neri P, Bahlis NJ, Nooka AK, Dhodapkar MV, Jaye DL, et al. Multiple myeloma immunoglobulin lambda translocations portend poor prognosis. Nat Commun 2019;10(1):1911 doi 10.1038/s41467-019-09555-6. [PubMed: 31015454]
41. Consortium EP. An integrated encyclopedia of DNA elements in the human genome. Nature 2012;489(7414):57–74 doi 10.1038/nature11247. [PubMed: 22955616]
42. McCarty AS, Kleiger G, Eisenberg D, Smale ST. Selective dimerization of a C2H2 zinc finger subfamily. Mol Cell 2003;11(2):459–70 doi 10.1016/s1097-2765(03)00043-1. [PubMed: 12620233]
43. Velu CS, Chaubey A, Phelan JD, Horman SR, Wunderlich M, Guzman ML, et al. Therapeutic antagonists of microRNAs deplete leukemia-initiating cell activity. J Clin Invest 2014;124(1):222–36 doi 10.1172/JCI66005. [PubMed: 24334453]
44. O'Neil J, Grim J, Strack P, Rao S, Tibbitts D, Winter C, et al. FBW7 mutations in leukemic cells mediate NOTCH pathway activation and resistance to gamma-secretase inhibitors. J Exp Med 2007;204(8):1813–24 doi 10.1084/jem.20070876. [PubMed: 17646409]
45. Reynolds TC, Smith SD, Sklar J. Analysis of DNA surrounding the breakpoints of chromosomal translocations involving the beta T cell receptor gene in human lymphoblastic neoplasms. Cell 1987;50(1):107–17 doi 10.1016/0092-8674(87)90667-2. [PubMed: 3036364]
46. Hirschhorn JN, Brown SA, Clark CD, Winston F. Evidence that SNF2/SWI2 and SNF5 activate transcription in yeast by altering chromatin structure. Genes Dev 1992;6(12A):2288–98 doi 10.1101/gad.6.12a.2288. [PubMed: 1459453]
47. Peterson CL, Herskowitz I. Characterization of the yeast SWI1, SWI2, and SWI3 genes, which encode a global activator of transcription. Cell 1992;68(3):573–83 doi 10.1016/0092-8674(92)90192-f. [PubMed: 1339306]
48. Olsson A, Venkatasubramanian M, Chaudhri VK, Aronow BJ, Salomonis N, Singh H, et al. Single-cell analysis of mixed-lineage states leading to a binary cell fate choice. Nature 2016;537(7622):698–702 doi 10.1038/nature19348. [PubMed: 27580035]

Author Manuscript Author Manuscript Author Manuscript Author Manuscript

Implications

Combinatorial diversity and cooperation between DNA binding proteins and complexes assembled by them can direct context-dependent transcriptional outputs to control cell fate and may offer new insights for therapeutic targeting in cancer.

Author Manuscript Author Manuscript Author Manuscript Author Manuscript

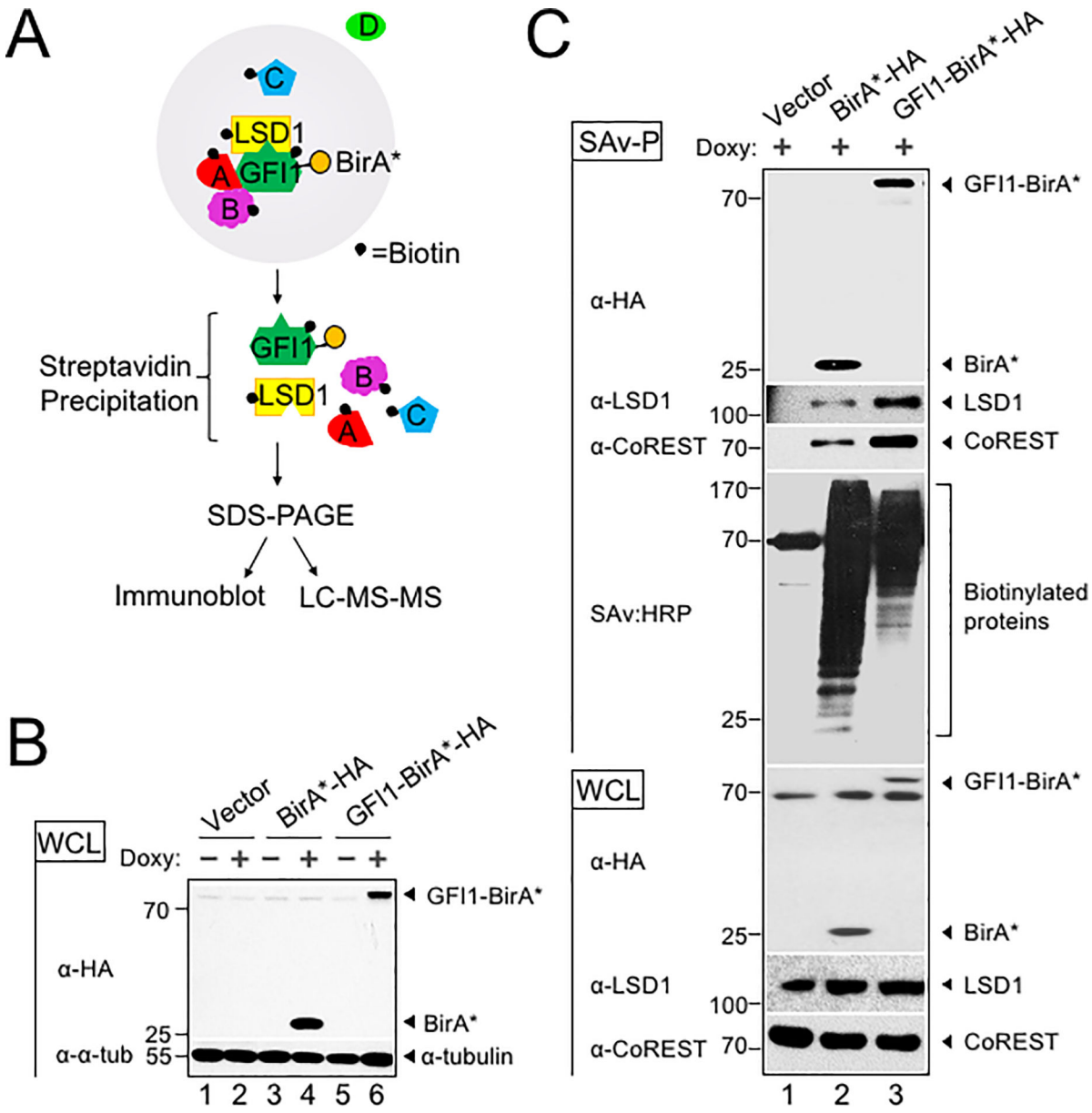

Figure 1.

BioID proximity labeling identifies GFI1-interacting proteins. (**A**) Scheme for BioID proximity labeling method to identify GFI1-proximate proteins. Gray circle reflects the radius for biotinylation of nearby molecules such as GFI1 itself and its known binding partner LSD1, as well as unknown proteins A, B and C but not D. (**B**) CCRF-CEM cells inducibly express BirA*-HA alone or as a fusion with GFI1. Biotin-treated CCRF-CEM cells transduced with empty vector (lanes 1–2), BirA*-HA (lanes 3–4), or GFI1-BirA*-HA (lanes 5–6) were treated with doxycycline (Doxy) (+) or vehicle control (−). Whole cell lysates (WCL) were resolved by SDS-PAGE and immunoblotted using HA antibodies. α-tubulin is shown as a loading control. (**C**) Biotinylation of GFI1-associated proteins LSD1 and CoREST is enriched using GFI1-BirA*-HA expressing CCRF-CEM cells relative to empty vector or BirA*-HA controls. Whole cell lysates prepared as in (B) were used

for immunoblotting or were first precipitated using streptavidin Sepharose beads (SAv-P), and subsequently analyzed by immunoblotting with anti-HA, anti-LSD1 or anti-CoREST antibodies, or streptavidin-HRP (SAv:HRP) to detect biotinylation.

Author Manuscript Author Manuscript Author Manuscript Author Manuscript

Author Manuscript Author Manuscript Author Manuscript Author Manuscript

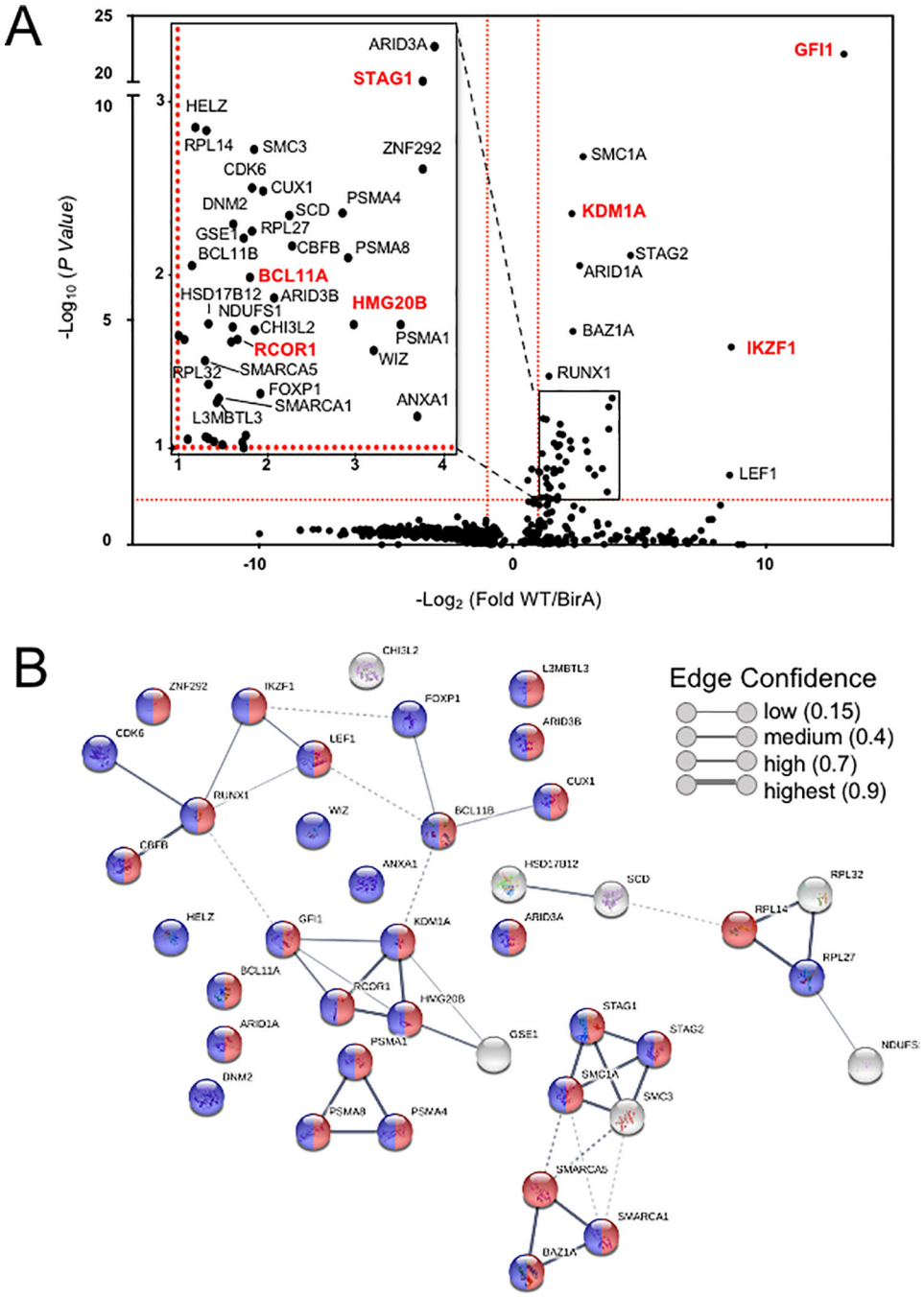

Figure 2.

Top hits of GFI1 proximal partners identified by proteome-wide BioID labeling. (**A**) Volcano plot of proteins identified by BioID proximity labeling. Thresholds (red dashed lines) were fold-difference >2 and *P*-value <0.05. (**Inset**) Magnified portion of (A) depicting significant hits. Known GFI1 partners and GFI1 itself are labeled in red. (**B**) Genes labeled in (A) were subjected to STRING (version 10.5) functional protein association network analysis. Edges represent protein—protein associations. Blue indicates annotated nuclear proteins. Red indicates annotated proteins associated with gene regulation. The network was

clustered using the MCL algorithm with inflation parameter 3. Dotted line indicates the proteins belong to different clusters.

Author Manuscript Author Manuscript Author Manuscript Author Manuscript

Author Manuscript Author Manuscript Author Manuscript Author Manuscript

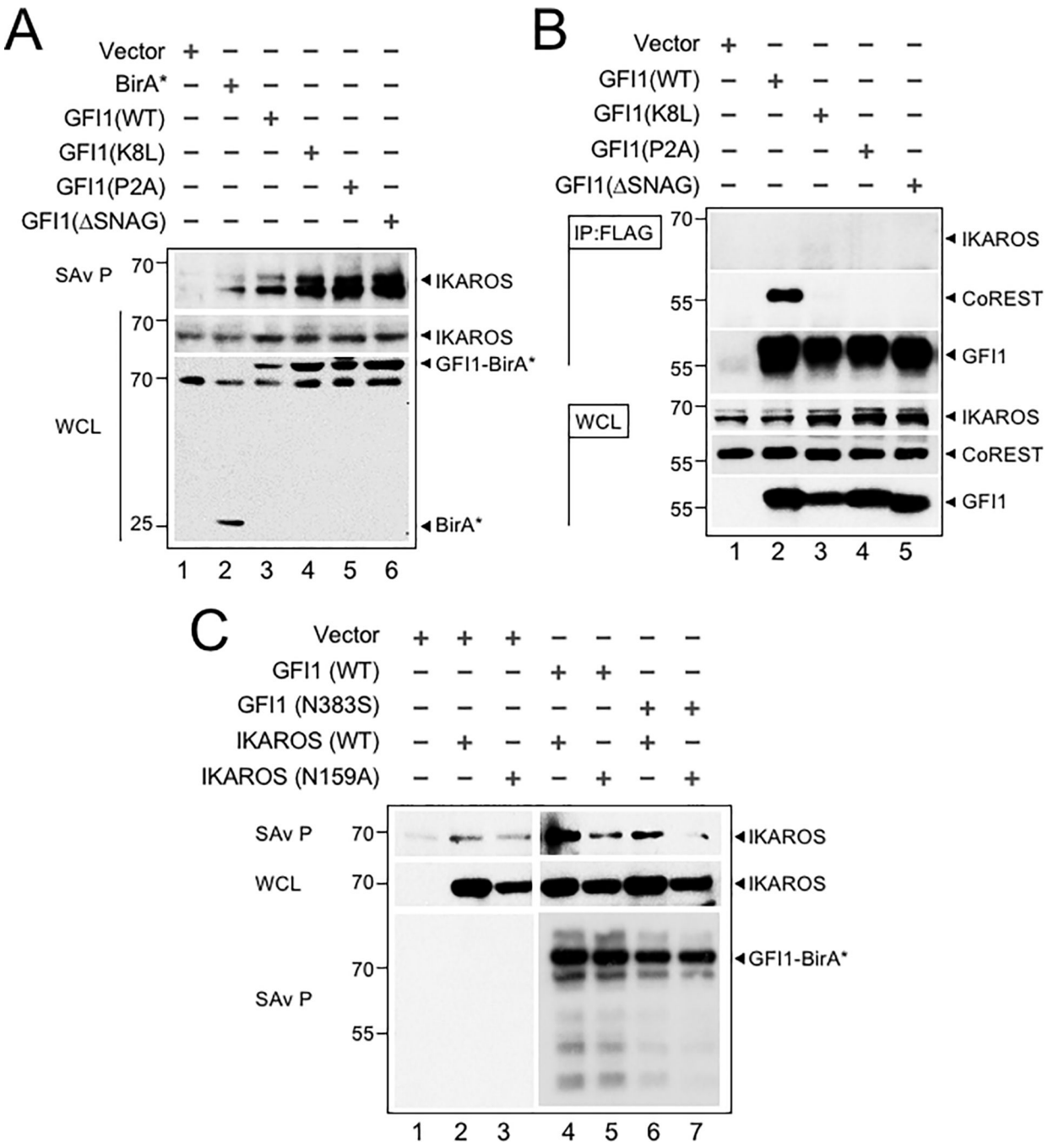

Figure 3.

The GFI1—IKAROS interaction requires DNA binding. (**A**) Validation and non-LSD1 binding dependence of the GFI—IKAROS proximity relationship. Biotinylated proteins in whole cell lysates from CCRF-CEM cells transduced with the indicated constructs and treated as in Figure 1B were isolated with streptavidin beads and immunoblotted with anti-IKAROS and anti-HA antibodies targeting the epitope tag in GFI1-BirA* fusion protein variants. (**B**) GFI1—IKAROS binding is not observed in traditional coprecipitation methods. Lysates from CCRF-CEM cells inducibly expressing wild type GFI1–3×FLAG or variants

Author Manuscript Author Manuscript Author Manuscript Author Manuscript

(K8L,P2A and ΔSNAG) were immunoprecipitated with anti-FLAG antibody and Protein G-Sepharose. The presence or absence of IKAROS, CoREST, or GFI1 in the precipitate was detected by immunoblotting with anti-IKAROS, anti-CoREST or anti-FLAG antibodies. 2% input whole cell lysate (WCL) is shown as a control. (**C**) The proximity relationship between GFI1 and IKAROS requires DNA binding activity of both proteins. HEK293T cells were transiently transfected with empty vector or GFI1-BirA*-HA (wild type or N383S) together with human IKAROS-3×FLAG (wild type or N159A) expression constructs. IKAROS and control GFI1 biotinylation was monitored by precipitation with streptavidin beads and IKAROS immunoblotting as described in panel A. A GFI1 immunoblot is shown to confirm equivalent precipitation with streptavidin-Sepharose beads.

Author Manuscript Author Manuscript Author Manuscript Author Manuscript

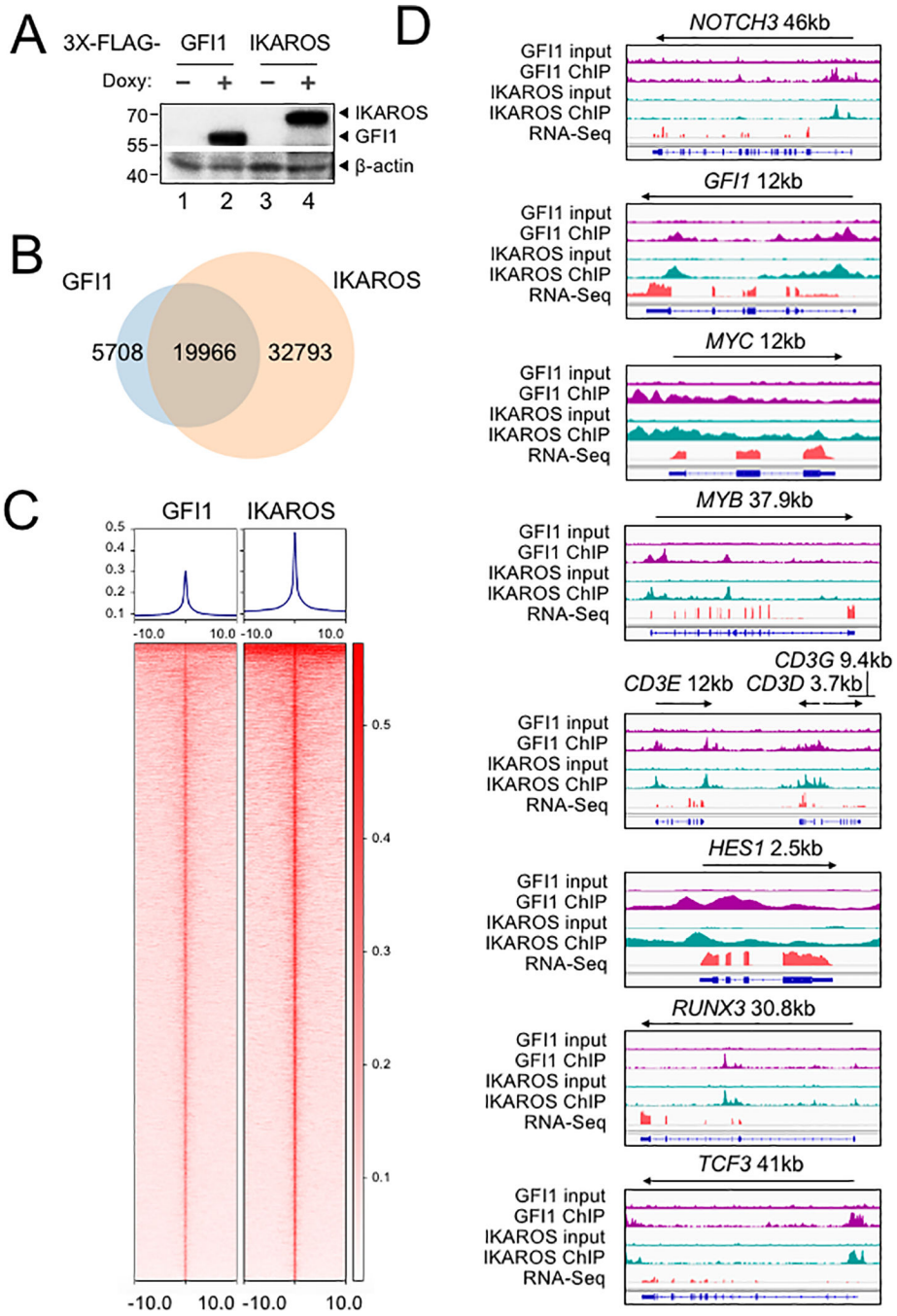

Figure 4.

Identification of GFI1 and IKAROS targets in CCRF-CEM cells. (**A**) Validation of GFI1 and IKAROS expression in CCRF-CEM cell lines by Western blotting. CCRF-CEM cells expressing GFI1–3×FLAG and IKAROS-3×FLAG were used for ChIP-Seq. (**B**) Venn diagram showing enumeration of unique and shared GFI1 and IKAROS ChIP-Seq peaks. (**C**) Left: GFI1 ChIP-Seq heatmap showing all peak sites, centered by the ChIP peak summit and arranged from strongest to weakest. Right: the same set of peak summits in the same order shown as an IKAROS binding heatmap. (**D**) Example Integrative Genomics Viewer

Author Manuscript Author Manuscript Author Manuscript Author Manuscript

(IGV) tracks of GFI1 ChIP-Seq and input controls (purple), IKAROS ChIP-Seq and input controls (teal), together with previously published RNA-Seq (peach) of CCRF-CEM cells. *NOTCH3*, *GFI1*, *MYC*, *MYB*, *CD3*, *HES1*, *RUNX3* and *TCF3* tracks are shown.

Author Manuscript Author Manuscript Author Manuscript Author Manuscript

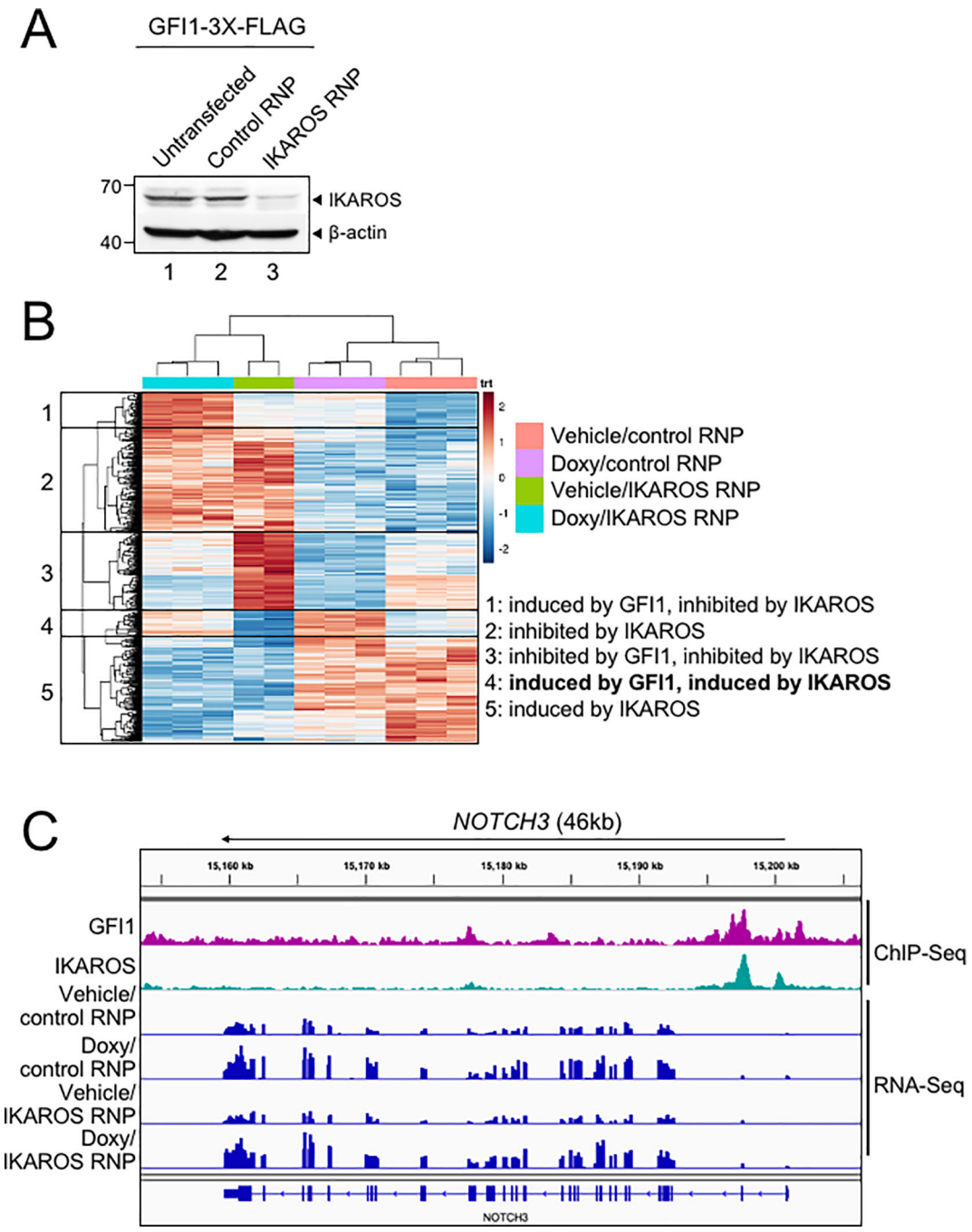

Figure 5.

GFI1 and IKAROS positively regulate a subset of target genes. (**A**) IKAROS Western blot of untransfected CCRF-CEM-GFI1–3×FLAG cells, cells electroporated with ATTO550-conjugated control or *IKZF1*-specific RNPs. 24 hr post-transfection, ATTO550^{+} cells were sorted and cultured for 9 additional days prior to preparation of lysates. β-actin is shown as a loading control. (**B**) RNA-Seq analysis was performed using the same control RNP- or *IKZF1*-specific RNP-transfected cells shown in (A) after treatment with vehicle or doxycycline (Doxy) for 24 hr. The top 500 differentially expressed genes (based on *P*-value)

Author Manuscript Author Manuscript Author Manuscript Author Manuscript

were subjected to hierarchical clustering and are shown as a heatmap. Gene groupings with distinct expression patterns (1–5) are highlighted. (**C**) IGV tracks displaying GFI1 and IKAROS ChIP-Seq and RNA-Seq read distribution for *NOTCH3*.

Author Manuscript Author Manuscript Author Manuscript Author Manuscript

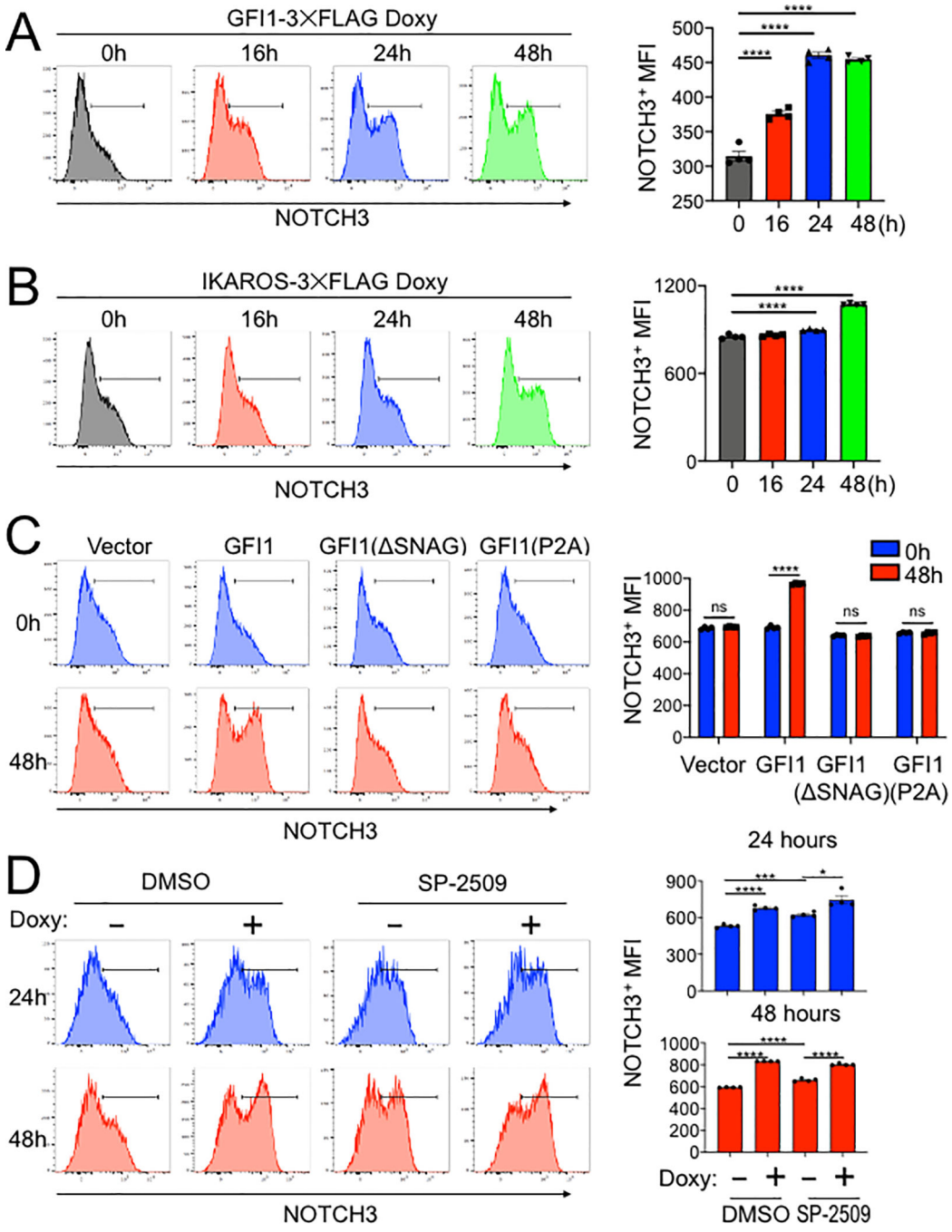

Figure 6.

IKAROS cooperates with GFI1 to regulate cell surface NOTCH3 protein expression. (**A**) Left: example flow cytometry histograms showing NOTCH3 surface expression in CCRF-CEM-GFI1–3×FLAG cells treated with doxycycline (Doxy) for the indicated times. Untreated (0 hr) cells are shown as a control. Right: NOTCH3 MFIs from cells in the regions highlighted in the left panels were averaged from four experiments and plotted as a bar graph. Bar colors match the corresponding histograms. Error bars depict SEM. Ordinary one-way ANOVA was used for statistical analysis. In all bar graphs, values for individual

Author Manuscript Author Manuscript Author Manuscript Author Manuscript

data points are represented by closed shapes. (**B**) Left: CCRF-CEM-IKAROS-3×FLAG cells were treated with doxycycline for the indicated times. Example NOTCH3 flow cytometry histograms are shown. Right: NOTCH3 MFIs from four independent experiments were averaged and plotted as in (A). Error bars depict SEM. Ordinary one-way ANOVA was used for statistical analysis. (**C**) CCRF-CEM cells transduced with empty vector (V), wild type GFI1–3×FLAG (GFI1), FLAG-tagged GFI1 lacking the N-terminal SNAG domain (ΔSNAG) or FLAG-tagged GFI1 with a SNAG domain point mutant no longer able to interact with LSD1 (P2A). Cells were treated with vehicle (blue) or doxycycline (red) for 48 hr. Left: representative flow cytometry histograms for NOTCH3 cell surface expression. Right: average MFIs from four independent experiments. Error bars depict SEM. Two-way ANOVA was used for statistical analysis. (**D**) Flow cytometry of CCRF-CEM-GFI1–3×FLAG cells pre-treated with DMSO vehicle or LSD1 inhibitor (1 μM SP-2509, MedKoo Biosciences) for 20 hr and subsequently treated with doxycycline for 24 or 48 hr. DMSO or SP-2509 was present continuously. Left: representative NOTCH3 flow cytometry. Right: MFIs within the NOTCH3-positive gates were averaged from four independent experiments and plotted as a bar graph. Error bars depict SEM. An unpaired T-test was used for statistical analysis.

Author Manuscript Author Manuscript Author Manuscript Author Manuscript

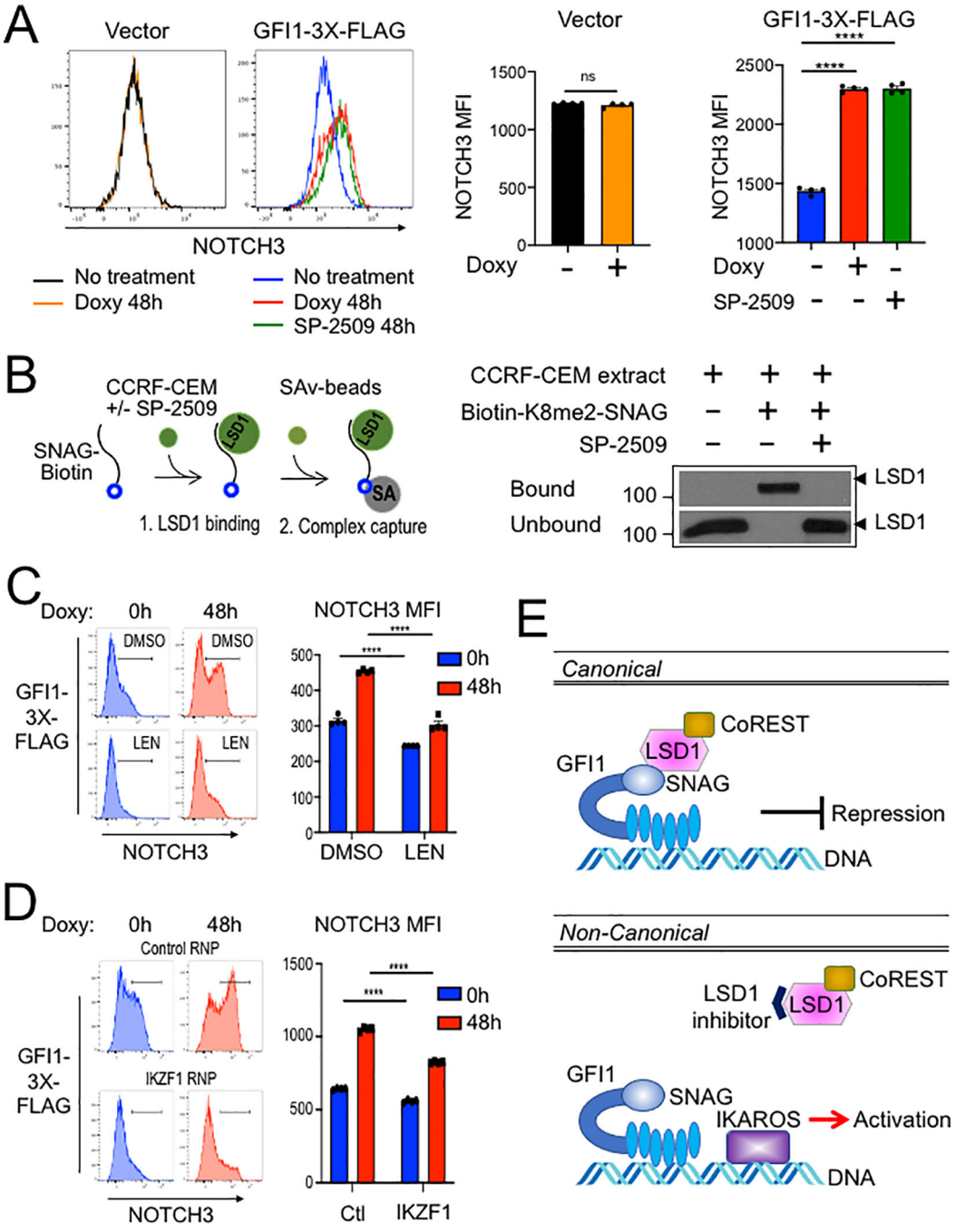

Figure 7.

(**A**) Flow cytometry for NOTCH3 cell surface expression in SUP-T1cells transduced with vector or GFI1–3×FLAG inducible vectors and treated without or with doxycycline (Doxy), and SP-2509 for 48 hr. Left: representative NOTCH3 flow cytometry. Right: NOTCH3 MFIs were averaged from four independent experiments and plotted as a bar graph. Error bars depict SEM. An unpaired T-test was used for statistical analysis. In each bar graph, values for each independent test are represented by closed shapes. (**B**) SP-2509 abolishes the SNAG—LSD1 interaction. Biotinylated SNAG peptide demethylated at K8 was added to

Author Manuscript Author Manuscript Author Manuscript Author Manuscript

CCRF-CEM cell extracts with or without SP-2509 and incubated for 1hr prior to addition of streptavidin-Sepharose beads to collect biotinylated peptide and bound LSD1. LSD1 in the bound and unbound fractions were visualized by western blot using anti-LSD1 antibody. (**C**) Flow cytometry of CCRF-CEM-GFI1–3×FLAG cells pretreated with DMSO or 2 μM lenalidomide (LEN) for 16 hr before treatment with doxycycline for 48 hr. DMSO or Lenalidomide was present continuously. Left: example NOTCH3 flow cytometry. Right: MFIs within the NOTCH3-positive regions shown at left were averaged from four independent experiments and plotted as a bar graph. Bar color corresponds to histogram shading on the left. Error bars depict SEM. Error bars depict SEM. Two-way ANOVA was used for statistical analysis. (**D**) Flow cytometry of CCRF-CEM-GFI1–3×FLAG cells electroporated with control RNP or *IKZF1* RNPs as in Figure 5A. Cells were treated with doxycycline for 0 or 48 hr. Left: example NOTCH3 flow cytometry. Right: MFIs within the NOTCH3-positive regions shown on the left were averaged from four independent experiments and plotted as a bar graph. Error bars depict SEM. Two-way ANOVA was used for statistical analysis. (**E**) A proposed model for GFI1-mediated non-canonical transcriptional activation. In the well-known canonical transcriptional regulation mechanism, GFI1 acts as a transcriptional repressor by recruiting LSD1/CoREST-containing complexes via its SNAG domain. In non-canonical transcriptional activation, GFI1 activates *NOTCH3* and other hallmark T cell developmental genes with IKAROS. DNA binding by both proteins is required, as is an intact SNAG domain not bound by LSD1. An LSD1 inhibitor, which blocks SNAG—LSD1 binding enables transactivation of *NOTCH3* and similarly regulated genes via the GFI1—IKAROS partnership.